Publ. Astron. Soc. Japan 29, 1-25 (1977)

A Computational and Observational Study of Peculiar Galaxies in the Coma Cluster

Mitsuaki FUJIMOTO and Yoshiaki SOFUE

Department of Physics, Nagoya University, Nagoya 464

and

Jun JUGAKU

Tokyo Astronomical Observatory, University of Tokyo, Mitaka, Tokyo 181

(Received 1976 April 5; revised 1976 October 15)

Abstract

Expected numbers of elliptical galaxies distorted tidally in the Coma cluster are formulated in terms of the various parameters of the cluster, and of cross section of galaxy-galaxy encounters and duration of associated tidal distortions. For the latter two quantities, numerical computations are carried out by simulating elliptical galaxies with hundreds of test particles. Comparisons are made with the number of peculiar galaxies observed in the Coma cluster. The hypothesis that the "missing mass" of the Coma cluster is hidden in the form of invisible galaxies or huge black holes of ordinary galaxy masses is also tested. It is concluded that tidal interaction between the visible galaxies plays only a minor role in the origin of the peculiar galaxies in the Coma cluster. Most of them would be due to their individual non-tidal mechanisms. If invisible galaxies or massive black holes are assumed as cluster members, their encounters with the luminous members increase the frequency of observable tidal distortion, and approximately half of the number of the peculiar galaxies could be explained in terms of tidal interaction. This result is discussed in relation to some special types of the peculiar galaxies in the Coma cluster.

Key words: Coma cluster; Missing mass; Peculiar galaxy; Tidal interaction.

1. *Introduction*

The Coma cluster has been studied extensively by many authors from various points of view, and many important problems have already arisen: The "missing mass" associated with dynamical structure, radio and X-ray emissions, supergiant ellipticals or cD galaxies, and diffuse luminous material at the cluster center. These problems must be, of course, related to each other, but many trials searching for underlying physics are still dispersed and fragmentary.

Among them, the "missing mass" problem, or the discrepancy between the

virial and luminous masses in clusters of galaxies, remains to be solved ever since it was first recognized by Zwicky (1933). In particular for the Coma cluster, many observations seem to have confirmed that the cluster is indeed stable dynamically, and that the total mass is of the order of that inferred from the application of the virial theorem: The ratio of the virial to the luminous masses is about 7 (this ratio will be henceforth referred to as γ) for the mass-to-luminosity ratio $M/L=30$ in solar units (Rood et al. 1972). A variety of proposals have already been made to solve this discrepancy in mass, but no ultimate interpretation seems to have been obtained yet. See Field (1972), Tarter and Silk (1974), and references cited therein for the historical and current status of investigations in this field.

In the present paper we examine whether the peculiar galaxies in the Coma cluster can be attributed to tidal interactions among the luminous member galaxies. Also we test the hypothesis that all of the missing mass of the Coma cluster is due to invisible galaxies or to huge black holes of ordinary galaxy masses. Here we suppose that ingredients of the invisible galaxies are dwarf stars, cold stars, and/or black holes associated with the final state of stellar evolution.

The procedures are to calculate the expected number of elliptical galaxies distorted by the encounters with visible and invisible galaxies, and to compare it with the number of peculiar galaxies in the cluster.

2. *Expected Number of Tidally Distorted Galaxies*

Figure 1 shows the observed luminosity-frequency function of member galaxies within 11.2 of the center of the Coma cluster (Rood 1969). When the mass-luminosity ratio, M/L, is constant within the cluster, it also represents the mass function of member galaxies which we shall use in the present paper. For later convenience in numerical computations, the member galaxies are divided into six

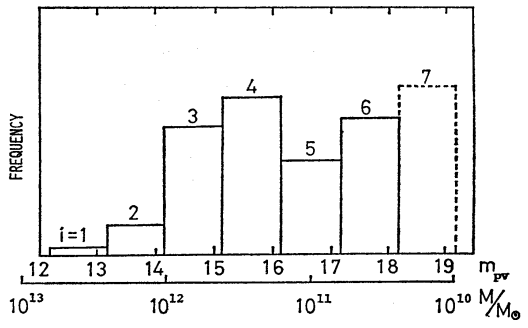

Fig. 1. The luminosity-frequency function of galaxies within 11.2 of the center of the Coma cluster (Rood 1969). For convenience of numerical calculations, it is represented in a histogram with columns $i=1$ to 7. When the mass-luminosity ratio is the same for all members, this histogram represents just a mass-frequency function, which we use throughout the present paper. The second abscissa is given in solar mass units for $M/L=30$, where a distance modulus of 35.7 mag ($H=50$ km s^{-1} Mpc^{-1}) and $m_{bol}-m_{pv}=0.9$ mag are adopted. The extreme right-hand column $i=7$ is an extrapolation of columns $i=1-6$.

groups, $i=1, 2, \cdots, 6$, according to their masses. Since energy equipartition is realized only partially among the members with different masses, we may take the following Maxwellian distribution with a common parameter σ.

$$n_i(r, \boldsymbol{v}_i)d\boldsymbol{v}_i = \frac{n_i^0(r)}{(2\pi\sigma)^3}\exp\left(-\frac{\boldsymbol{v}_i^2}{2\sigma^2}\right)d\boldsymbol{v}_i\,, \tag{1}$$

where $\boldsymbol{v}_i=(v_{ix}, v_{iy}, v_{iz})$, $i=1, 2, \cdots, 6$, and $n_i^0(r)$ is the number density of galaxies in the i-th group at a distance r from the cluster center. Of course, n_i^0's with $i=1$–6 are parallel to the mass spectrum in figure 1. The parameter σ is taken from the observed dispersion of the radial velocity, which is common to all the groups $i=1, 2, \cdots, 6$ and constant within the region of interest not far from the core ($r<50'$). The probability that two galaxies, one in the i-th group and another in the j-th group, encounter at a relative velocity $|\boldsymbol{v}_i-\boldsymbol{v}_j|$ is

$$P_{ij}d\boldsymbol{v}_i d\boldsymbol{v}_j = \frac{1}{[(2\pi)^{1/2}\sigma]^6}|\boldsymbol{v}_i-\boldsymbol{v}_j|\exp\left(-\frac{\boldsymbol{v}_i^2+\boldsymbol{v}_j^2}{2\sigma^2}\right)d\boldsymbol{v}_i d\boldsymbol{v}_j\,. \tag{2}$$

Introducing $\boldsymbol{v}_i-\boldsymbol{v}_j=\boldsymbol{V}$ and $\boldsymbol{v}_i+\boldsymbol{v}_j=\boldsymbol{U}$ into equation (2) and integrating over $\boldsymbol{U}$, we have

$$P_{ij}(V)dV = \frac{1}{(4\pi)^{1/2}\sigma^3}V^2\exp\left[-\left(\frac{V}{2\sigma}\right)^2\right]dV\,, \tag{3}$$

where $V=|\boldsymbol{V}|$. Then the number of encounters per unit time and unit volume is

$$\int_0^\infty n_i^0 n_j^0 (V\Omega_{ij})P_{ij}dV = \frac{1}{(4\pi)^{1/2}\sigma^3}n_i^0 n_j^0\int_0^\infty V^2(V\Omega_{ij})\exp\left[-\left(\frac{V}{2\sigma}\right)^2\right]dV\,, \tag{4}$$

where Ω_{ij} ($\neq\Omega_{ji}$) denotes the cross section for encounter between galaxies of the i-th and j-th group.

At the encounter the galaxy is tidally distorted. If observable distortion lasts for τ_{ij} ($\neq\tau_{ji}$), the number of distorted (peculiar) galaxies to be observed per unit volume is

$$n_{ij}^{\mathrm{dist}}(r) = \frac{8}{\pi^{1/2}}n_i^0 n_j^0\sigma\langle\Omega_{ij}\tau_{ij}\rangle\,, \tag{5}$$

where

$$\langle\Omega_{ij}\tau_{ij}\rangle = \int_0^\infty\left(\frac{V}{2\sigma}\right)^3\Omega_{ij}\tau_{ij}\exp\left[-\left(\frac{V}{2\sigma}\right)^2\right]d\left(\frac{V}{2\sigma}\right)\,. \tag{6}$$

The number density of member galaxies can be closely approximated by the following form (Rood et al. 1972):

$$n_i^0(r) = n_i^{00}/[1+(r/r_c)^2]^{3/2}\,, \tag{7}$$

where n_i^{00} is the number density of galaxies for the i-th group at the center and r_c is the scale length. Substituting equation (7) into equation (5) and taking into account that σ is independent of r, we have the expected total number of tidally distorted galaxies,

$$N^{\mathrm{T}}=\sum_{i,j}\int_0^\infty n_{ij}^{\mathrm{dist}}(r)4\pi r^2dr=2\pi^{3/2}\sigma r_{\mathrm{c}}^{\,3}\sum_{i,j}n_i^{00}n_j^{00}\langle\Omega_{ij}\tau_{ij}\rangle\,. \tag{8}$$

The number of distorted galaxies to be observed in the ring r–$r+dr$ on the sky is

$$C^{\mathrm{P}}dr=2\pi rdr\sum_{i,j}2\int_r^\infty\frac{n_{ij}^{\mathrm{dist}}(t)tdt}{(t^2-r^2)^{1/2}}$$
$$=\frac{6\pi^{3/2}r_{\mathrm{c}}^{\,6}r\sigma}{(r^2+r_{\mathrm{c}}^{\,2})^{5/2}}\sum_{i,j}n_i^{00}n_j^{00}\langle\Omega_{ij}\tau_{ij}\rangle dr\,. \tag{9}$$

In order to obtain numerical values for N^{T} and C^{P}, we must know the cross section Ω_{ij} and the duration of the observable tidal distortion τ_{ij}, which cannot be, however, described in an anayltic form. The following section is devoted to the evaluation of these quantities by numerical computations.

If the "missing mass" in the Coma cluster is due to invisible galaxies, and if their mass spectrum remains the same as in figure 1, then the observed number of tidally distorted (peculiar) galaxies is γ times N^{T} or C^{P} in equation (8) or (9). One of the principal aims of the present paper is to compare these numbers with observations.

Equations (2) to (9) have been derived on the basis of the Maxwellian distribution (1), which is consistent with the observed radial velocity distribution of Rood et al. (1972). Though no clear evidence exists for non-Maxwellian part in the velocity distribution, if a significant number of galaxies become in loosely bound pairs during the evolution of the cluster, a deviation from equation (1) would be unavoidable and leads to different conclusions. Therefore, we must remember that our conclusions in the present paper will be derived in our choice of the Maxwellian velocity distribution (1).

Table 1. Physical parameters used in the present computations.

The Hubble constant, H	50 km s^{-1} Mpc^{-1}
Distance to the Coma cluster, d	138 Mpc
Angular distance of 1′ at d=138 Mpc	0.0402 Mpc
Number density of galaxies at the cluster center, $\sum_i n_i^{00}$	150 Mpc^{-3}*
Scale length, r_{c}	6′ or 0.241 Mpc
Radial velocity dispersion, σ	1000 km s^{-1}
M/L	30 in solar units
Galaxy mass of m_{pv}=15.7 mag	$2.5\times10^{11}M_\odot$

* This number refers to galaxies brighter than m_{pv}=18.5 mag. When the Hubble constant was 100 km s^{-1} Mpc^{-1} and 75 km s^{-1} Mpc, they were respectively 1200 Mpc^{-3} (Omer et al. 1965) and 500 Mpc^{-3} (Rood et al. 1972).

The numerical values concerning the Coma cluster in table 1 are adopted throughout the present paper. For the Hubble constant we take H=50 km s^{-1} Mpc^{-1}. Some related discussions in the case of H=75 km s^{-1} Mpc^{-1} are made in the final section. Note in equation (8) that $r_{\mathrm{c}}\propto H^{-1}$ and $n_i^{00}\propto H^3$. The ratio of virial mass to luminous mass γ is independent of H for which we take γ=7 from Rood et al. (1972): $M_{\mathrm{vt}}\propto H^{-1}$ and $M_{\mathrm{lum}}\propto L(M/L)\propto H^{-2}(H^{-1}/H^{-2})\propto H^{-1}$.

3. *Tidal Interaction between Elliptical Galaxies*

3.1. *A Non-Rotating System of Particles as a Model for Elliptical Galaxies*

Tidal distortions of interacting disk galaxies have been extensively studied by simulating their continuous disk media by a number of test particles (Pfleider and Siedentopf 1961; Pfleider 1963; Yabushita 1971; Toomre and Toomre 1972; Wright 1972; Eneev et al. 1973; Clutton-Brock 1972; Fujimoto and Sofue 1976). In the present paper we will apply this method to tidal distortions of elliptical galaxies whose angular momentum per unit mass is thought to be small compared with that of spiral galaxies. We take a non-rotating system of test particles as a dynamical model for the outer portions of isolated elliptical galaxies. Since our interest is mainly in the overall features of the tidal distortion projected onto the orbital plane of two interacting ellipticals, we follow the two-dimensional motions of the particles distributed on this plane.

We assume the following Plummer's (1911) law for the potential of elliptical galaxies in the i-th group,

$$\Phi_i(\boldsymbol{\rho}-\boldsymbol{\rho}_i)=\frac{GM_i}{[(\boldsymbol{\rho}-\boldsymbol{\rho}_i)^2+a_i^2]^{1/2}}\ , \tag{10}$$

where M_i and $\boldsymbol{\rho}_i$ are the mass and the position vector of the galaxy center, and a_i is its typical radius. Within $|\boldsymbol{\rho}-\boldsymbol{\rho}_i|=a_i$ and $2a_i$ just fifty and eighty percent of the total luminosity are included, respectively, when projected onto the sky. In table 2 is shown an empirical relation between M_i and a_i taken from the data by Fish (1963).

Equations of orbital motion for the two interacting galaxies, i and j, in the inertial reference system, whose origin is at the center of mass, are written as

$$\ddot{\boldsymbol{\rho}}_i=\frac{\partial}{\partial\boldsymbol{\rho}_i}\Phi_j(\boldsymbol{\rho}_i-\boldsymbol{\rho}_j)\ , \tag{11}$$

and, of course,

$$M_i\boldsymbol{\rho}_i+M_j\boldsymbol{\rho}_j=0 \tag{12}$$

holds when $M_i=M_j$ and the closest approach of the two galaxies is sufficiently larger than a_i and a_j. In other cases we assume that a less massive galaxy moves as a point of the same mass in the field of a more massive galaxy of the Plummer-type potential (10). The equation of motion for a test particle is written as

$$\ddot{\boldsymbol{\rho}}=\frac{\partial}{\partial\boldsymbol{\rho}}\Phi_i(\boldsymbol{\rho}-\boldsymbol{\rho}_i)+\frac{\partial}{\partial\boldsymbol{\rho}}\Phi_j(\boldsymbol{\rho}-\boldsymbol{\rho}_j)\ , \tag{13}$$

Table 2. Representative mass and radius of elliptical galaxies.

Physical quantity	i						
	1	2	3	4	5	6	7
M_i (in $M_\odot$)	4×10^{12}	1.6×10^{12}	6.3×10^{11}	2.5×10^{11}	10^{11}	4×10^{10}	1.6×10^{10}
a_i (in kpc)*	12	6.7	3.5	2.1	1.0	0.6	0.4

* Taken from Fish (1964), thereby we use $H=50\,\mathrm{km\,s^{-1}\,Mpc^{-1}}$. Within the radii a_i and $2a_i$, just fifty and eighty percent of the total luminosity are observed.

where Φ_i and Φ_j are represented by the solutions of equations (11). Masses of the test particles and their mutual attraction are neglected.

Now we leave a number of rings of test particles to free radial oscillations in the potential (10), with amplitudes a_i–$2a_i$ in random phases. After a free-fall time, the oscillating rings result in an approximately steady state, realizing a smooth distribution and a velocity dispersion of free-fall motion. We take this state as a dynamical model for the outer portions of undisturbed elliptical galaxies. Approximately two hundred test particles are used in each elliptical galaxy.

3.2. *Parameters and Initial Conditions*

The perturbing body M_j is initially at $(X, Y)=(-200\,\mathrm{kpc}, p)$ with velocity $(V, 0)$, where (X, Y) is the coordinate system with its origin at the center of the perturbed galaxy M_i, and p denotes the impact parameter of the encounter. The velocity is also referred to this coordinate system. The time is reckoned from the pericenter passage or the closest approach of the two galaxies.

Masses of the interacting galaxies: We take a wide range of mass of the interacting galaxies, approximately from 10^{10} to $10^{13}\,M_\odot$. The mass interval is chosen so that it corresponds to one magnitude of luminosity, if M/L is constant. The representative galaxy mass of the i-th group is given in table 2.

Impact parameter: We classify the collisions according to the impact parameter p [head-on collision ($p=0$), close encounter ($p<2a_i$), and distant encounter ($p>2a_i$)].

Relative velocity: The observed dispersion of radial velocity is $1000\,\mathrm{km\,s^{-1}}$ in the central region of the Coma cluster, within $50'$ from the center. Then the relative velocity between two member galaxies is mostly 500–$3000\,\mathrm{km\,s^{-1}}$ with a maximum probability at $2000\,\mathrm{km\,s^{-1}}$ (section 2). Numerical computations were carried out at every $500\,\mathrm{km\,s^{-1}}$, or at $250\,\mathrm{km\,s^{-1}}$ if necessary. At these relative velocities, the orbits of two galaxies are highly hyperbolic.

3.3. *Results of the Numerical Computations*

Head-on collision: Figure 2 shows the behavior of the particles as a typical example of a head-on collision whose parameter combination is $(i, j; p, V)=(3, 3; 0\,\mathrm{kpc}, 1000\,\mathrm{km\,s^{-1}})$. Before the perturbing body M_j penetrates the galaxy M_i, no distortion of M_i is observed. Just after M_j passes the center of M_i, slight protuberances appear to form an elongated envelope along the line joining M_i and M_j. About 3×10^7 yr after the passage of M_j, a "fan"-shaped asymmetry appears simultaneously in the particle distribution at $|\boldsymbol{\rho}-\boldsymbol{\rho}_i|\approx a_i$. As time goes, the particles composing the fan return to the central region of M_i, penetrate through it, and make a similar fan appendage again on the side opposite to M_j. The fan-appendage structure oscillates in this way, decaying slowly due to the phase mixing of the particles. The period and lifetime of the oscillation are 5×10^7 and 3×10^8 yr, respectively.

The fan appendages are observed for most cases of head-on collision, oscillating back and forth for $(2\text{–}5)\times10^8$ yr. The appendage is more extended as the relative velocity becomes smaller and the perturbing body becomes more massive.

Further results are given in the Appendix, where we display the particle distributions in the cases of close and distant encounters. Also there is some dependence of our results on the adopted impact parameter, relative velocity, and perturbed galaxy mass.

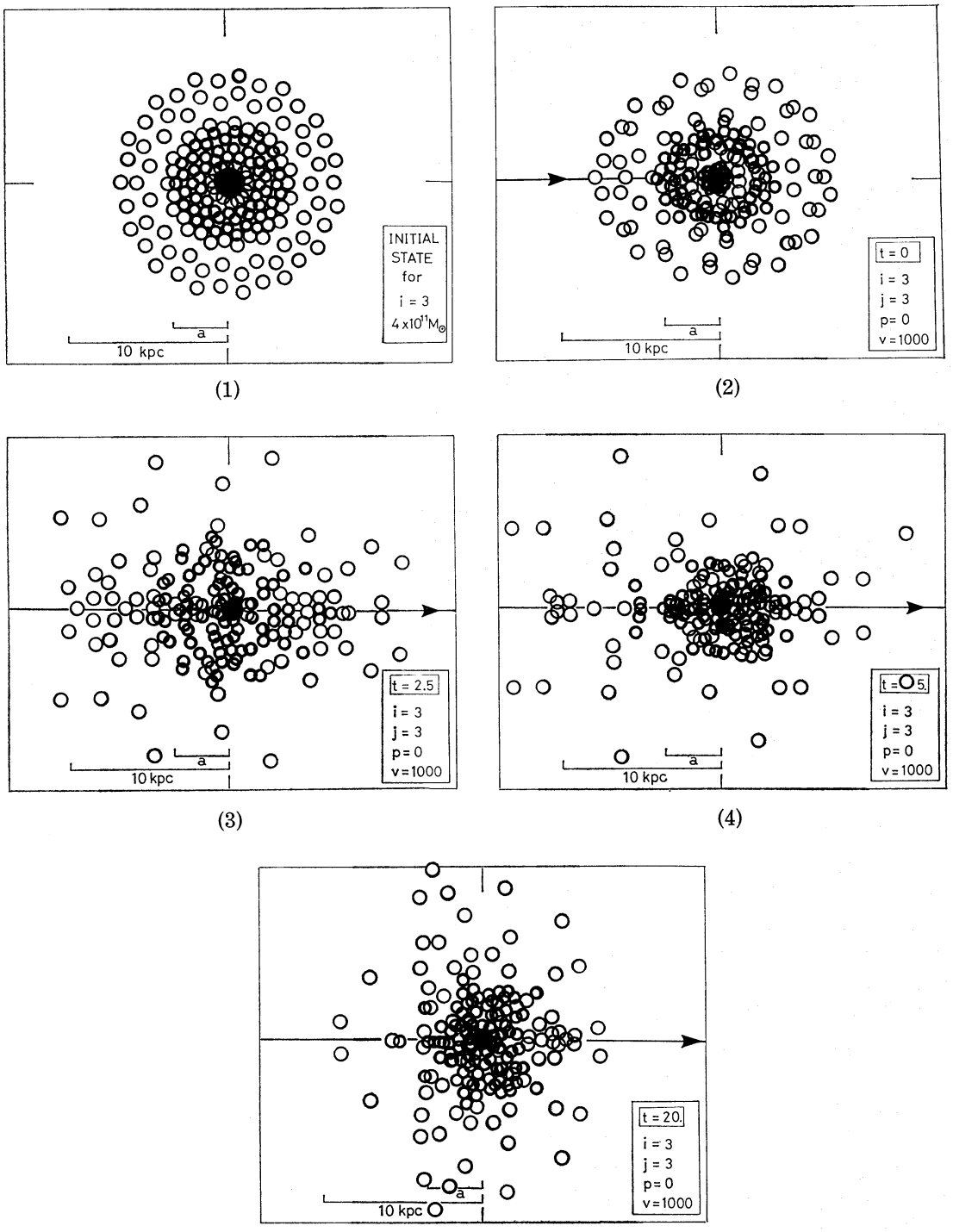

Fig. 2a. Initial distribution of the test particles in a model spherical galaxy and their behavior during a head-on collision with an equal mass galaxy; $(i, j; p, V)=$ (3, 3; 0 kpc, 1000 km s^{-1}). The small and large open circles indicate the positions of individual particles which had initial amplitudes of $\sim a_i$ and $\sim 2a_i$, respectively. The time is reckoned from the pericenter passage of the perturbing galaxy in units of 10^7 yr.

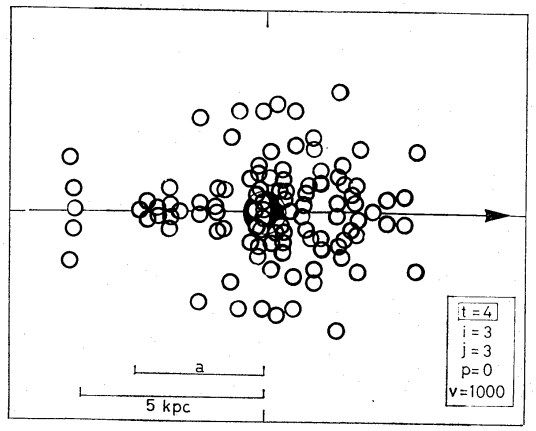

Fig. 2b. Same as figure 2a, but for the inner region $|\boldsymbol{\rho}-\boldsymbol{\rho}_i|\simeq a_i$ and $t=4\times10^7$ yr. Note the fan-shaped distribution of particles at $|\boldsymbol{\rho}-\boldsymbol{\rho}_i|\simeq a_i$, to which we shall refer as a fan-appendage.

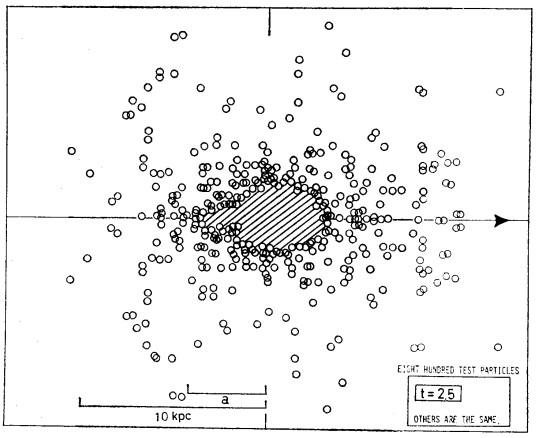

Fig. 2c. Same as the case of $t=2.5$ in figure 2a but the number of test particles is approximately eight hundred. The hatched area around the center is a region where the test particles are too crowded to be distinguished one from the other. In both figures is seen an elongated distribution of particles along the orbit of the perturbing galaxy.

The parameters that we adopted here cover $i=1$ to 6, $j=1$ to 6, $p=0$ to 80 kpc with every 5 kpc and $V=0$ to 5000 km s^{-1} with every 500 km s^{-1} (or 250 km s^{-1} if necessary). Since combinations of these parameters are too many, we were forced by computer facilities to deal with our numerical simulations with approximately two hundred test particles. In order to examine whether this number is too small and statistical fluctuations in particle distribution would exaggerate the deformations, we tried the same simulations in some cases with eight hundred particles. Two results are given as examples in figures 2c and A1e, in which the hatched areas indicate the regions in which many particles are distributed too densely to be distinguished separately. Comparisons with the distributions of two hundred test particles at the corresponding time reveal no essential difference between them. We can regard, therefore, the following numerical results as being sufficiently quantitative in a frame of our test particle simulation.

3.4. *Data for Determining* τ_{ij} and Ω_{ij}

Cross section and duration of the tidal interaction can be determined from an eye-estimate of the distribution of the test particles in figures 2 and A1 to A3 in the Appendix. Some basic data for such determinations are given for nine cases of $i, j=1, 3, 5$ in figure 3a, where the abscissae and ordinates indicate the relative velocity V (in km s^{-1}) and the impact parameter p (in kpc), respectively. Encounters of two model galaxies, i and j, cause "observable" distortions of the model galaxy i, when p and V are taken below the curved line in the (i, j)-box, where the term "observable" stems from an eye-estimate of the particle distribution. Numerals along the curved lines in figures 3b–c designate the duration of the observable distortion measured in units of 10^7 yr. Simultaneouly, the impact parameter p along these lines enables us to compute the cross section $\Omega_{ij}\cong\pi p^2$ as a function of V. Substituting the products of Ω_{ij} and τ_{ij} into equation (6), we can evaluate $\langle\Omega_{ij}\tau_{ij}\rangle$.

The symbols A, F, E, and J in figure 3a are used to represent characteristic features observed at the maximum distortion in the particle distribution. The meanings are introduced below and are illustrated on the top of figure 3a.

A; Asymmetric distribution: Overall elongated and bar-like distortions, whose major axis is 1.5 or more times as large as the minor axis.

J; Jet: When the perturbing galaxy is massive and the relative velocity is not so large, a jet-like protuberance appears, lasting about 5×10^7 yr or less. The jet is not necessarily directed to the perturbing galaxy (see figure A1b).

F; Fan-shaped distribution: The test particles extend in an asymmetric way in many cases, like a fan with an opening angle of 60° to 180° (see figures 2, A2). This type of model galaxy will be compared with the "fan-appendage" peculiar galaxies.

E; Extended envelope: Almost axisymmetric (spherically symmetric) expansion of the test particles (see figure A7c).

Detailed comparisons between some special types of observed peculiar galaxies and our distorted model galaxies will be made in the next section. Thereby it

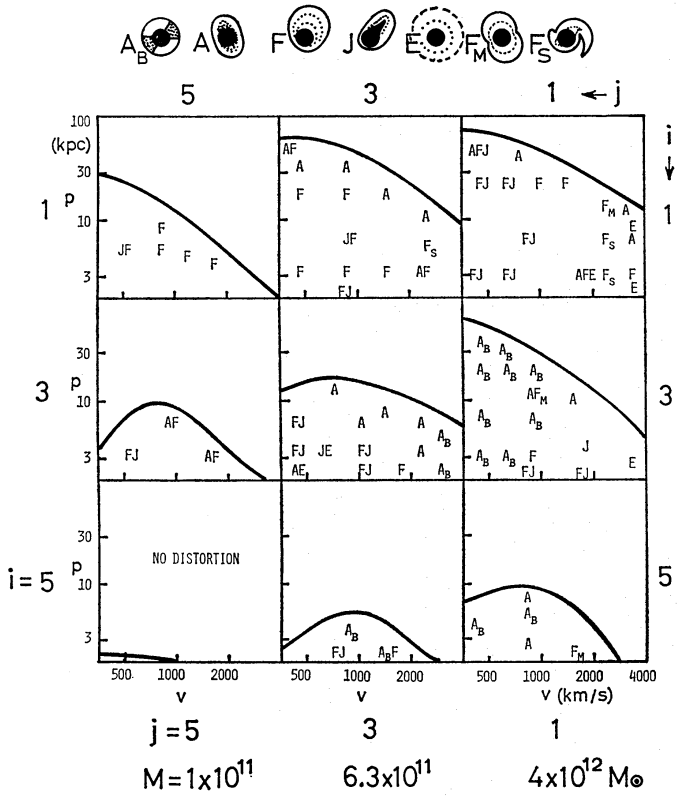

Fig. 3a. Various types of "observable" tidal distortions for the impact parameter p, relative velocity V, and $i, j=1$, 3, and 5. Morphological meanings of symbols A, F, J and E are given atop of the figure and in the text. When p and V are taken below the curved line in each (i, j)-box, the "observable" distortions readily occur, where the term "observable" stems from an eye estimate of the distribution of the test particles in figures 2a-c. The durations τ_{ij} for A and E are approximately equal to those for F given in figure 3b.

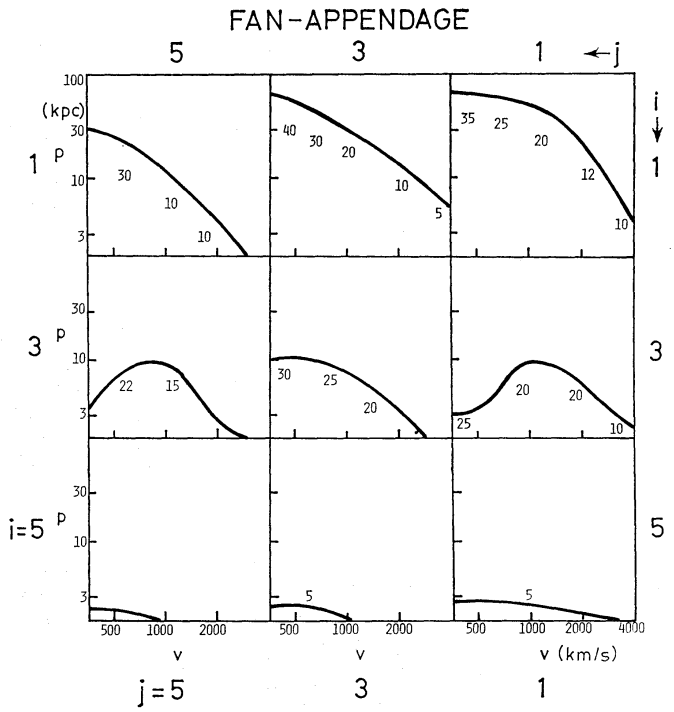

Fig. 3b. Same as figure 3a, but only for the fan-type distortion. Numerals along each curved line are durations of the tidal distortion measured in units of 10^7 yr. Along this line, we can evaluate the cross section ($\Omega_{ij} \simeq \pi p^2$) and duration ($\tau_{ij}$) as a function of V in each (i, j)-box.

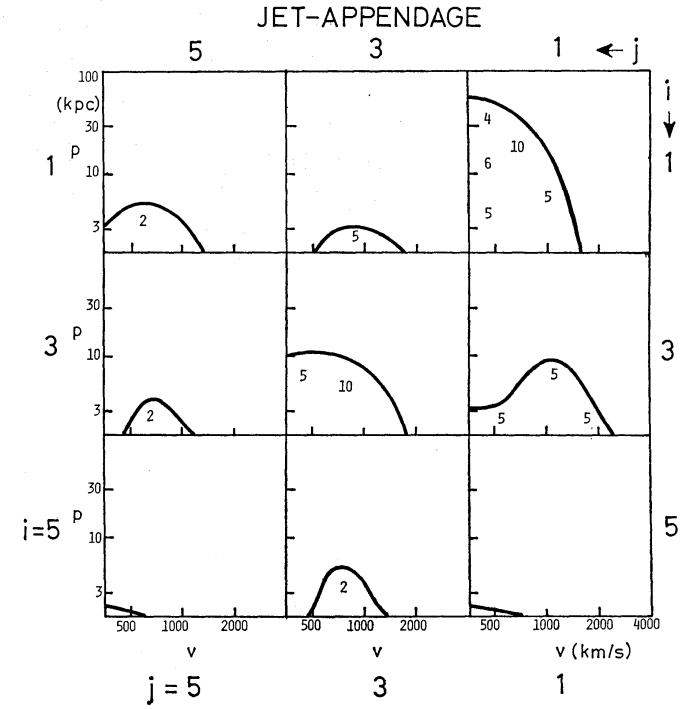

Fig. 3c. Same as figures 3a and 3b, but only for the jet-type distortion.

proves convenient to know Ω_{ij} and τ_{ij} for each of these types. For this purpose, the basic data for F and J in figure 3a are separately given in figures 3b and 3c.

4. *Comparison with Observations*

4.1. *Observations*

Rood (1968) identified a number of peculiar galaxies within 20′ from the center of the Coma cluster, and classified them according to their apparent characteristics: supergiant scale, close double, bridge, tail, jet-appendage, and fan-appendage. Table 3 lists these peculiar galaxies. Figure 4a gives their distribution on the sky as a function of distance from the center of Coma cluster.

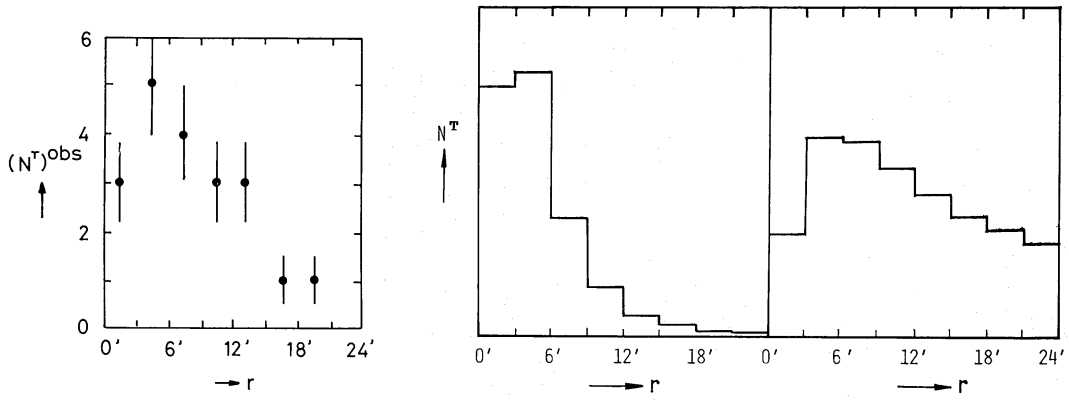

(a) (b) (c)

Fig. 4. (a) Observed frequency distribution of peculiar galaxies in the rings circled by $r-1'.5$ and $r+1'.5$ on the sky. The peculiar galaxies with asterisks in table 3 are not included, because they were detected in our survey within only 15′ from the center of the cluster. Each bar represents statistical error. (b) Theoretical distribution law of tidally distorted elliptical galaxies. The abscissa is the same as in figure 4a. (c) Projection of the distribution law of galaxies, equation (7), onto the sky. The areas of the histograms in figures 4b and 4c are not the same.

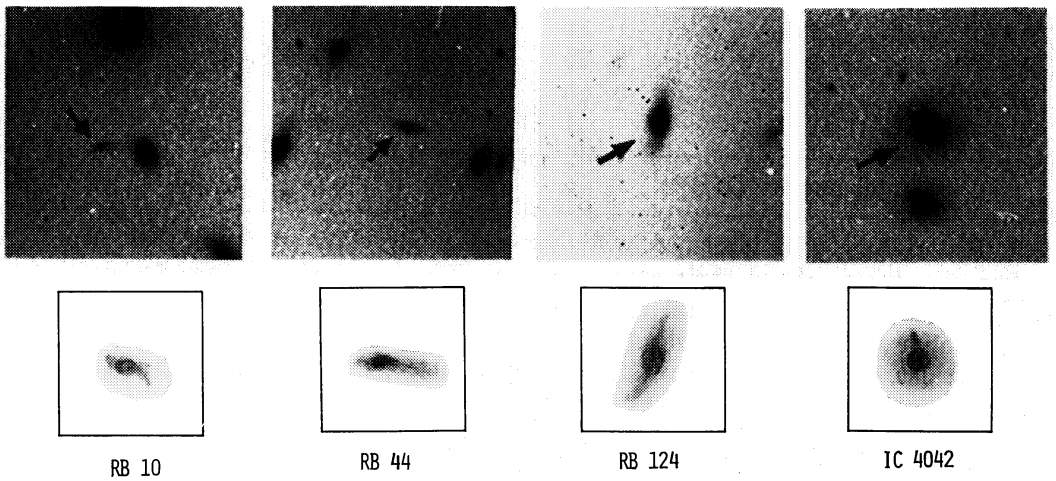

Fig. 5. Enlarged photographs of newly identified peculiar galaxies near the center of the Coma cluster; viz, RB 10, RB 44, RB 124, and IC 4042. North is the top and east to the left. Scale: 1 cm=0′.54. Also given are schematic illustrations of their characteristic shapes.

In order to add more information about distorted galaxies, we photographed the central region of the Coma cluster on a baked IIIa-J plate in a 2-hr exposure at the Newtonian focus of the 188-cm reflector at the Okayama Astrophysical Observatory. From a detailed examination of our deeply exposed plate as well as of the Palomar Sky Survey prints, we found four other distorted or asymmetric galaxies within 15′ of the cluster center. They are the galaxies numbered as RB 10, RB 44, and RB 124 in the Rood and Baum (1967) list of the Coma cluster members, and IC 4042. We also included these galaxies in table 3.

Table 3. List of peculiar galaxies in central region of the Coma cluster (Rood 1968).

Galaxy	Angular distance	Morphological type	Rood type	Case		
				I	II	III
RB 71	2′.4	E	J	√	√	√
RB 75	3.0	E	J	√	√	√
RB 254	13.7		J	√	√	√
RB 36	6.7		F	√	√	√
RB 88	8.7		F	√	√	√
RB 197	24.1		F	√	√	√
RB 165	17.2		F	√	√	√
NGC 4895	15.2	S0p	MB	√		
RB 39	7.4	S0	MB	√		
IC 4040	11.4	I/SC	MB	√		
NGC 2898	5.8	E E	CD	√√		
RB 142-143	9.2	E E	CD	√√		
RB 220-218	12.5		CD	√√		
RB 64-65	2.5	SB0	O	√√	√√	
RB 56	3.5		O	√	√	
RB 33	5.2	E	O	√	√	
IC 3949	14.8	S0p	O	√	√	
RB 10*	7.5	S0	Bending	√		
RB 44*	6.8	S0	Jet toward the west	√		
RB 124*	14.9	S0	Bending	√		
IC 4042*	11.1	E	Jet or knots	√		
Total number $(N^{T})^{obs}$				25	12	7

* Distorted galaxies identified by the present study. Except for IC 4042 they show peculiar structures only at their outer portions. They are excluded from the data in detailed comparison with theoretical results (Cases II and III).

A peculiar galaxy with the symbol CD is counted as two in our statistics (see below).

(1) J: Jet, F: Fan appendage, MB: Multiple buldge, CD: Close double, and O: other. These terms are due to Rood (1968).

(2) Peculiar structures characterized by MB and CD could not be reproduced by the present particle simulations. In a detailed comparison with theoretical results, they are excluded from the data. The galaxies designated by the symbol √ are counted in Cases I, II, and III.

(3) Since peculiar structures with J and F could be well reproduced by the computer simulation, we make a most reliable comparison on the basis of the data in Case III.

Figure 5 shows enlarged pictures of these galaxies. RB 10 is a lenticular galaxy as seen edge-on, east and west edges of which are bent to the north and to the south, respectively. RB 44 is a lenticular galaxy unusually elongated toward the west. RB 124 is a normal lenticular galaxy, but shows a slight bending toward the east on its southeast end. IC 4042 is a spherical S0 galaxy, but has a small protuberance emerging from the central bulge toward the north-northeast.

Some of these galaxies are slightly distorted only at their outer parts, not so conspicuous as those in Rood's (1968) list, but they could contribute to the data on tidally distorted galaxies.

4.2. *Comparison between Observations and Numerical Results*

If all or some of the peculiar galaxies in table 3 are due to tidal interactions between visible galaxies, the numbers in the last row are to be compared with N^{T} in equation (8). Furthermore, if invisible galaxies or massive black holes exist as cluster members and contribute to the missing mass, the number of tidally distorted galaxies is expected to increase to γN^{T}. Here we assume that the invisible members have a mass spectrum parallel to that of the luminous members in figure 1.

(i) Before entering into detailed comparison with observations, we try to obtain rough numbers of N^{T} and γN^{T}, using the constants in table 1. Here we shall use the units of 1 Mpc for length, 1000 km s^{-1} for velocity, and approximately 10^9 yr for time. In equation (8), we have $\sigma \approx 1$, $r_c \approx 1/4$, $\sum_{i,j} n_i^{00} n_j^{00} \approx 4 \times 10^4$ and then $2\pi^{3/2} \sigma r_c^3 \sum_{i,j} n_i^{00} n_j^{00} \cong 10^4$. We tentatively take $\Omega_{ij} \cong \pi(0.03)^2$ for $p=0.03$, and $\tau_{ij} \cong 0.2$ (a typical free-fall time). From a simple behavior of the function $x^3 \exp(-x^2)$ in equation (6) with $x = V/2\sigma$, we can get roughly $\langle \Omega_{ij}\tau_{ij} \rangle \cong 5 \times 10^{-5}$ by substituting $\Omega_{ij}\tau_{ij} \approx 6 \times 10^{-4}$ into equation (6). Consequently, the product of these numbers yields $N^{\mathrm{T}} \cong 0.5$, and $\gamma N^{\mathrm{T}} \cong 3.5$ when $\gamma = 7$.

So far as the total number N^{T} is concerned, the tidal interaction seems only a minor agency causing peculiar phenomena in the galaxies. When invisible members are included, the expected total number of distorted galaxies increases up to $\gamma N^{\mathrm{T}} \cong 3.5$. However, it is still smaller than the number of peculiar galaxies in Case I of table 3 by a factor of 7. If this factor is reduced close to unity in the following detailed calculations, we could get support for the existence of invisible galaxies in the Come cluster.

(ii) More reliable conclusions, of course, should be derived on the basis of more exact values of the cross section and duration of tidal interactions for which we have carried out the model computations in wide ranges of galaxy mass, impact parameter, and relative velocity.

We assume here that all of the tidally distorted model galaxies of A, F, J, and E types in table 3 correspond more or less to the observed peculiar galaxies in the Coma cluster. Then we sum up $\langle \Omega_{ij}\tau_{ij} \rangle$ over i and j, and also over all types of distortions A, F, J, and E. After straightforward numerical calculations, we obtain

$$(N^{\mathrm{T}})_{\mathrm{A+F+J+E}} \cong 0.3\,, \quad \text{and} \quad \gamma(N^{\mathrm{T}})_{\mathrm{A+F+J+E}} \cong 2.1 \text{ for } \gamma = 7\,. \tag{14}$$

These numbers are rather smaller than those estimated roughly in (i), and are far smaller than in Case II of table 3. We conclude again that most of the peculiar galaxies in the Coma cluster are due not to tidal interaction but to some

mechanism intrinsic to each individual galaxy.

In order to see this conclusion in a different light, we present in figure 4c a projection of equation (9) onto the sky. If the peculiar galaxies are caused by their individual mechanisms, their frequency distribution must be parallel to that of equation (7) projected onto the sky (figure 4c). Actually the distribution law (figure 4a) is in between figures 4b and 4c.

(iii) As demonstrated in figure 2 and in figures in the Appendix, ordinary oblate ellipticals and the tidal distortions classified as A and E look so much alike that it might be practically impossible to distinguish one from the other. It seems, therefore, better to exclude A- and E-type distortions from our following detailed comparison. On the other hand, some types of peculiar galaxies in table 3, multiple bulges and close doubles in Rood's (1968) terms, could not be reproduced by any means in the present test-particle simulation. They are probably beyond the present simple dynamical approach. We may exclude these two types from our data. As mentioned in section 2, we have evaluated Ω_{ij} and τ_{ij} by viewing the particle distributions at $a_i<|\boldsymbol{\rho}-\boldsymbol{\rho}_i|<2a_i$. We therefore exclude from our discussions the peculiar galaxies with asterisks in table 3; only their extended envelopes show asymmetric features.

Now we are left with types F and J in our computed tidal distortions, and with the two types of peculiar galaxies with "fan-appendage" and "jet" in Case III in table 3. From equation (5) and figures 3a–c we have

$$(N^{\mathrm{T}})_{\mathrm{F+J}}\cong 0.24\ ,\quad \text{and}\quad \gamma(N^{\mathrm{T}})_{\mathrm{F+J}}\cong 1.7\ \text{for}\ \gamma=7\ , \tag{15}$$

or, more specifically,

$$(N^{\mathrm{T}})_{\mathrm{F}}\cong 0.2\ ,\quad \text{and}\quad \gamma(N^{\mathrm{T}})_{\mathrm{F}}\cong 1.4\ \text{for}\ \gamma=7\ , \tag{16}$$

and

$$(N^{\mathrm{T}})_{\mathrm{J}}\cong 0.04\ ,\quad \text{and}\quad \gamma(N^{\mathrm{T}})_{\mathrm{J}}\cong 0.3\ \text{for}\ \gamma=7\ . \tag{17}$$

Again we find all of these values are smaller than the numbers of "fan appendage" and "jet" in Case III in table 3. The conclusions derived in (i) and (ii) remain valid also in this fine analysis.

However, $\gamma(N^{\mathrm{T}})_{\mathrm{F}}$ in calculation (16) differs from the number of the corresponding peculiar galaxies by a factor of only 3. This difference seems still large but it is much reduced compared with other cases. Its meaning will be touched on in the final section.

5. *Conclusions and Discussion*

Using the numerically-computed cross section of galaxy–galaxy collisions and the duration of the associated tidal distortions, we have obtained $N^{\mathrm{T}}\approx 0.3$ as the expected number of tidally distorted elliptical galaxies in the Coma cluster. This number is far smaller than that of the peculiar galaxies, $(N^{\mathrm{T}})^{\mathrm{obs}}\approx 10$ to 20, in the central region of the cluster ($r<20'$), and leads us to the conclusion that most of the peculiar galaxies are due not to tidal interaction but to some individual mechanism in each galaxy. Hereafter we use the symbol $(\ )^{\mathrm{obs}}$ to indicate observed values.

Even if we increase the collision frequency by a factor of $7(=\gamma)$ by assuming invisible galaxies as cluster members, the expected number of distorted galaxies

is still too small, i.e., $\gamma(N^{\mathrm{T}})\cong 2.1$.

From the numbers of known distorted members with and without visible companions in the Virgo cluster, van den Bergh (1969) inferred that collapsed objects with masses of 10^8 to $10^{13}\,M_\odot$ are less frequent than luminous galaxies are in the Virgo cluster, and that their contribution to the missing mass is only minor. However, if both the collapsed objects and visible members are in random motions in the overall gravitational field of the cluster, their mutual encounters are hyperbolic. The statistical estimate must be made by fully taking into account both the cross section and duration of the tidal interaction. At least in the Coma cluster, we cannot rule out the existence of a huge amount of invisible galaxies or black holes as the missing mass.

The most reliable comparison is made between the F-type model ellipticals and the observed peculiars with fan appendages; i.e., $\gamma(N^{\mathrm{T}})_{\mathrm{F}}\cong 1.4$ and $(N^{\mathrm{T}})^{\mathrm{obs}}_{\mathrm{fan\,appendage}}=4$. The difference between these two numbers is not so large as to devastate the hypothesis on the missing mass, but it seems rather in favor of it. Indeed, if we take into account the self-gravity of the test particle, the F-type distortion would last longer as a coherent oscillation, and the above discrepancy by a factor of 3 would be reduced, perhaps, to a factor of 2 or less.

We have adopted $H=50\,\mathrm{km\,s^{-1}\,Mpc^{-1}}$ so far. If we use a still-often-quoted value $H=75\,\mathrm{km\,s^{-1}\,Mpc^{-1}}$, the expected number of tidally distorted galaxies becomes 3.4 $[=(75/50)^3]$ times the present value in equation (14) or $(N^{\mathrm{T}})_{\mathrm{A+F+J+E}}=0.3\times 3.4=1$ [see also equation (8)], which leads us to the same conclusion on the tidal origin of the peculiar galaxies. However, our hypothesis on the missing mass becomes more reasonable for $\gamma=7$ or $M/L=30$ (Rood et al. 1972). Indeed, from equation (14) we obtain $\gamma(N^{\mathrm{T}})_{\mathrm{A+F+J+E}}=7\times 0.3\times(75/50)^3=7$, almost half of the number of the peculiar galaxies in Case II in table 3. When we restrict our statistics to the model galaxies of F-type distortion, we obtain $\gamma(N^{\mathrm{T}})_{\mathrm{F}}=5$, which is nearly equal to the number of the fan-appendage peculiar galaxies. In either case of $H=75$ or $50\,\mathrm{km\,s^{-1}\,Mpc^{-1}}$, it is still difficult to verify the present hypothesis but there are some observational indications which are not inconsistent with the hypothesis.

We have estimated thus far the number of tidally distorted elliptical galaxies on the basis of Ω_{ij} and τ_{ij} computed for a non-rotating particle system. Even if we try the same kind of computation for a slightly rotating system or disk system simulating a flat galaxy, the present conclusions would remain unchanged; as we have discussed in section 2, the mean relative velocity between the member galaxies is as large as $2000\,\mathrm{km\,s^{-1}}$, approximately ten times a typical rotation velocity of the system, and thus the distortion and its duration do not change so drastically compared with those of a non-rotating system.

All computations were made on a HITAC 8500 at the Institute of Plasma Physics, Nagoya University. We are indebted to Professor K. Takayama, Director of the Institute, for making the computer available to us.

Appendix. *Numerical Computations of Galaxy Encounters*

We have shown in figure 2 an example of our numerical computations for the parameter combination, $(i, j; p, V)=(3, 3; 0\,\mathrm{kpc}, 1000\,\mathrm{km\,s^{-1}})$. In this appendix we discuss further results and display more examples of the particle distributions

in cases of close and distant encounters. As well, we examine some dependence of the results on the collision parameters. Also discussed are variations of angular momentum and total energy of the perturbed galaxy during the encounter.

Close encounter ($p<2a_i$)

Figure A1 gives a result for the close encounter of equal-mass galaxies and the parameters $(i, j; p, V)=(3, 3; 5\,\mathrm{kpc}, 1000\,\mathrm{km\,s^{-1}})$ in which $p=1.5a_i$. In this case the dynamical situation is qualitatively the same as in the head-on collision in figure 2, but a jet-like protuberance takes place at $t=5\times10^7$ yr in the opposite direction to the galaxy having passed nearby. This transient structure lasts only for some 5×10^7 yr. Furthermore, we observe that the galaxy undergoes an overall asymmetric deformation, resulting in an elongated shape with axial ratio of roughly 1:1.5. This feature lasts for a relatively longer time, 2×10^8 yr. Figure A1e is the result for eight hundred test particles, corresponding to the former case of $t=5$. A similar jet-like protuberance is recognized in both computations.

Distant encounter ($p>2a_i$)

Figure A2 shows a typical example of the time development of the tidal distortion of a medium-mass galaxy. The adopted parameters are $(i, j; p, V)=(3, 1; 20\,\mathrm{kpc}, 1000\,\mathrm{km\,s^{-1}})$, in which $p=5.7a_i$. A fan-appendage appears and lasts for roughly 3×10^8 yr. Also is observed a formation of spiral protuberance at $t=2.5\times10^7$ yr, which soon disappears into an elongated irregular distribution.

Figure A3 shows the encounter for the same parameters as in figure A2, except for a larger impact parameter, $p=30\,\mathrm{kpc}=8.6a_i$. In this case, a slight deformation takes place only in the outer region of the galaxy. In cases of more distant encounters, or $p>50$ kpc and $V>1000\,\mathrm{km\,s^{-1}}$, no distortion is observed.

Dependence on impact parameter

In figure A4 we display the distribution of the test particles for encounters between equal-mass galaxies. Various impact parameters are taken, $p=0$, 50, 20, and 30 kpc, while other parameters are fixed at $(i, j; V)=(3, 3; 1000\,\mathrm{km\,s^{-1}})$. The tidal deformation is more pronounced as the impact parameter decreases. No significant distortion is observed for $p>30$ kpc.

Dependence on relative velocity

The particle distributions are followed in a medium-mass galaxy in head-on collision with a more-massive galaxy, $(i, j; p)=(3, 1; 0)$. Figure A5 shows three cases for $V=500$, 1000, and $1500\,\mathrm{km\,s^{-1}}$, in which we find that deformations are not so sensitive to the relative velocity. On the other hand, we display in figure A6 the particle distributions for the cases of $(i, j; p)=(1, 1; 30\,\mathrm{kpc})$, which depend sensitively on the relative velocity: The model galaxy $i=1$ is largely deformed when $V=500$ to $750\,\mathrm{km\,s^{-1}}$, whereas it suffers only slight damages for $V>1200\,\mathrm{km\,s^{-1}}$. These two facts in figures A5 and A6 are in agreement with the tidal distortion being proportional to $1/V^2D^4$ as predicted from the impact approximation of Spitzer (1957), where D is the perigalactic distance in the binary encounters.

Mass dependence

Figure A7 shows the tidal deformation for various masses of the perturbed galaxy, $i=1, 3$, and 5, where other parameters are fixed; $(j; p, V)=(1; 20\,\mathrm{kpc}, 1000\,\mathrm{km\,s^{-1}})$. It is somewhat surprising that the deformation is more pronounced in more massive galaxies. This tendency is due to the smaller pericenter distance realized when the perturbed galaxy is more massive, and also due to the fact

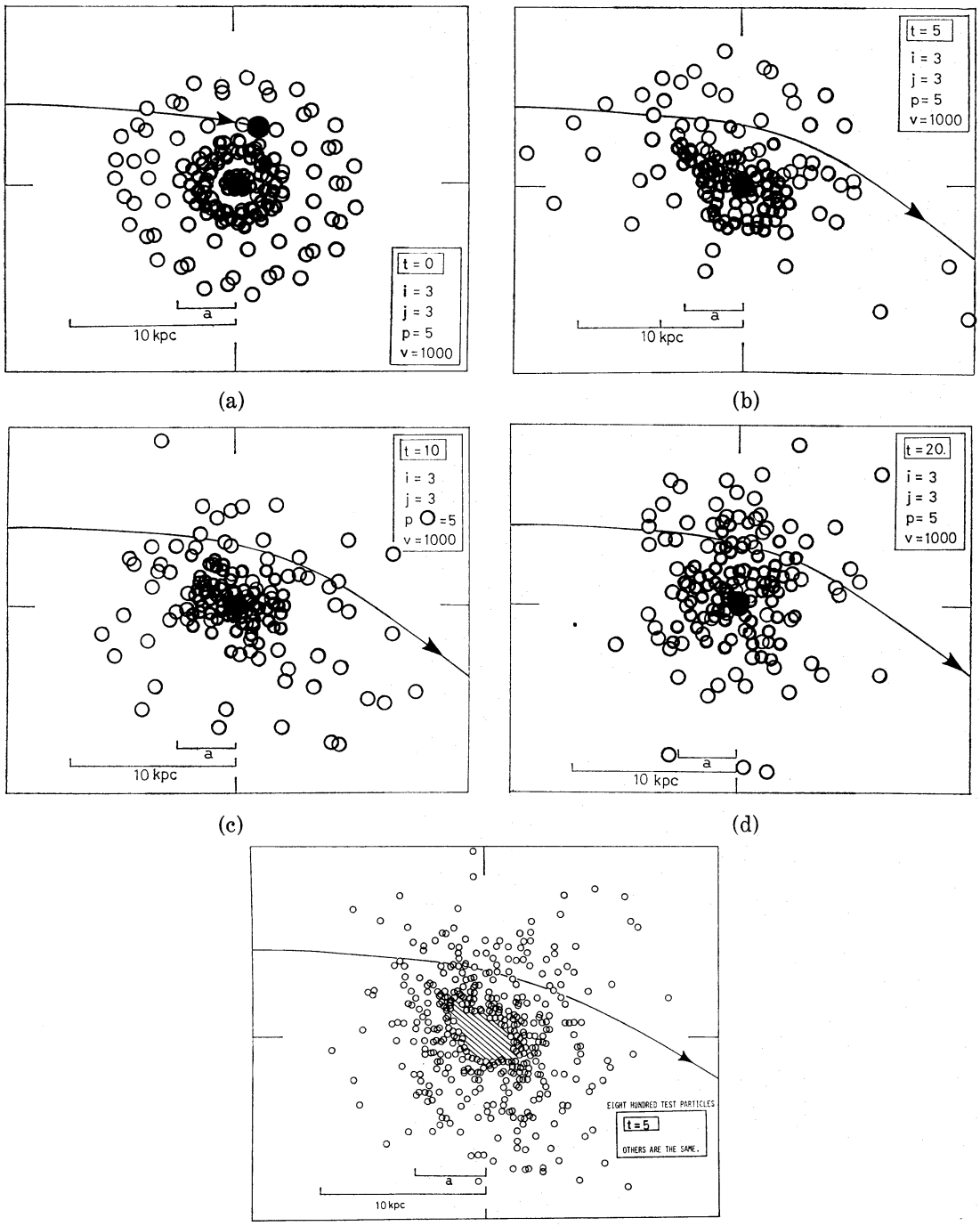

Fig. A1. Distributions of the test particles in a model spherical galaxy with $M_i = M_j = 6.3\times10^{11}\,M_\odot$. The parameters of this close encounter are $(i, j; p, V) = (3, 3; 5$ kpc, 1000 km s$^{-1})$. The small and large open circles indicate positions of the individual particles which had initial amplitudes of $\sim a_i$ and $\sim 2a_i$. The time is reckoned from the pericenter passage of the perturbing galaxy. The curved line indicates the orbit of the perturbing galaxy. At $t=5\times10^7$ yr, a jet-like protuberance is observed extending in the opposite direction to the galaxy having passed nearby. The large filled circles indicate the positions of the centers of the interacting galaxies.

Figure A1e is the same as that of $t=5$, but the number of the test particles is about eight hundred. A comparison of these two figures reveals no large difference in the characteristic distribution of the particles. In the hatched area many particles are distributed too densely to be plotted by individual open circles.

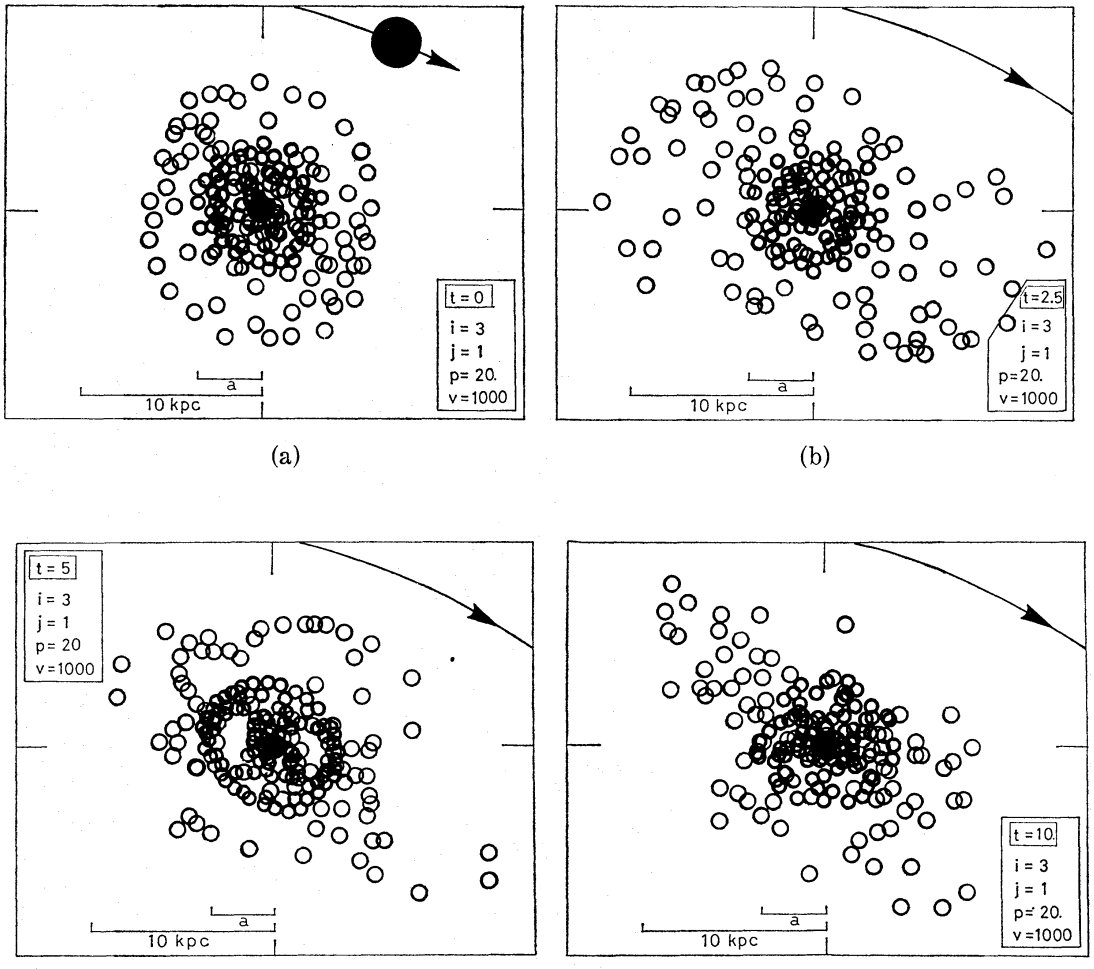

(a) (b)

(c) (d)

Fig. A2. Same as figure A1, but for a distant encounter at the impact parameter $p=20$ kpc$=5.7a_i$. The mass of the perturbing galaxy M_j is $4\times10^{12}M_\odot$, or $(i, j; p, V)=(3, 1; 20\text{ kpc}, 1000\text{ km s}^{-1})$.

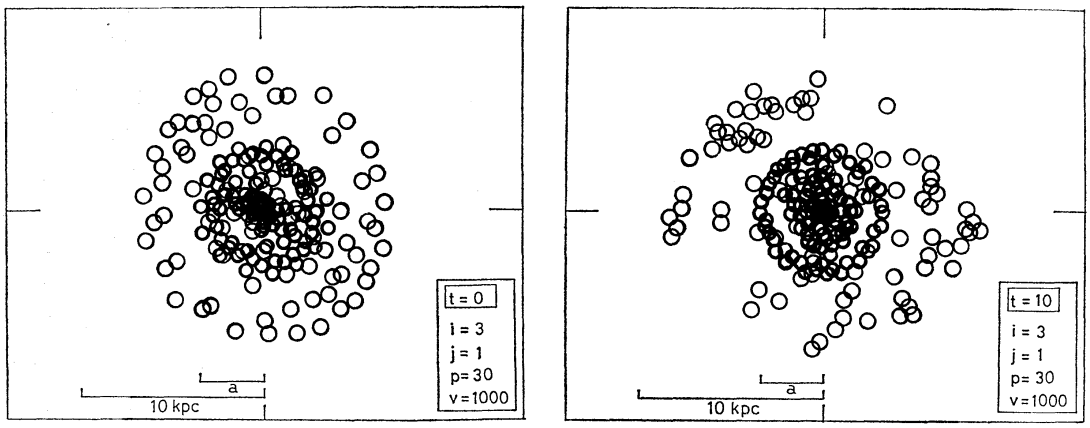

(a) (b)

Fig. A3a-b. See the legend on the next page.

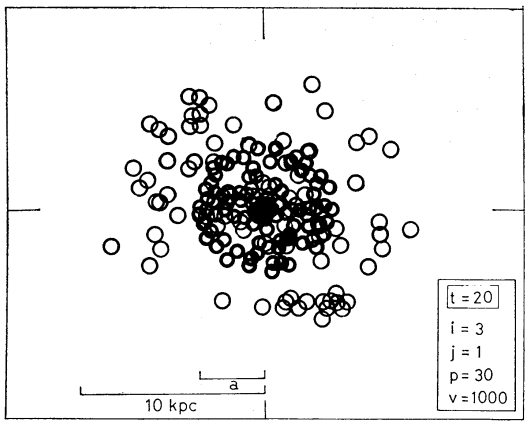

(c)

Fig. A3. Same as figure A2, but for the impact parameter $p=30$ kpc$=8.5a_i$, or $(i, j; p, V)=(3, 1; 30$ kpc, 1000 km s$^{-1})$.

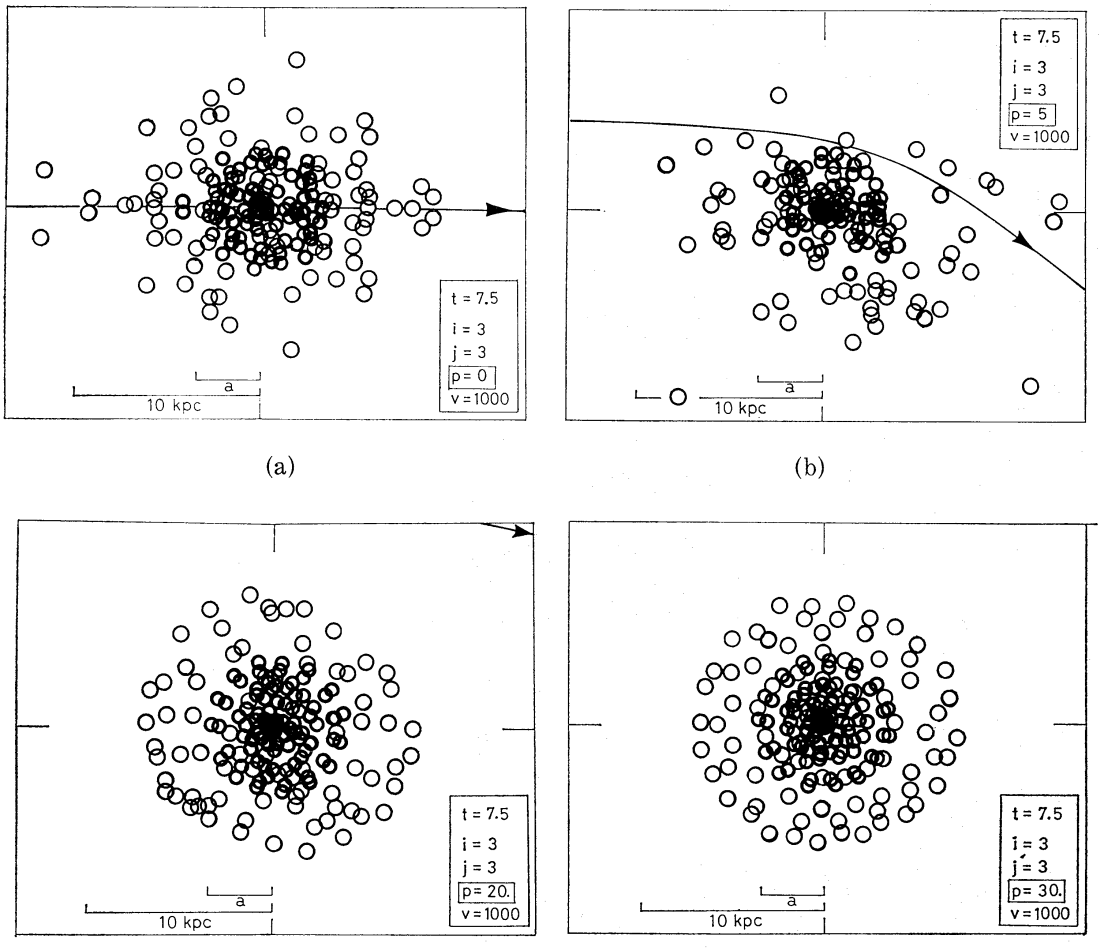

Fig. A4. Comparison of the particle distributions at $t=7.5\times10^7$ yr after an encounter with an equal-mass galaxy. The assumed impact parameters are $p=0$, 5, 20, and 30 kpc. Other parameters are fixed; $(i, j; V)=(3, 3; 1000$ km s$^{-1})$.

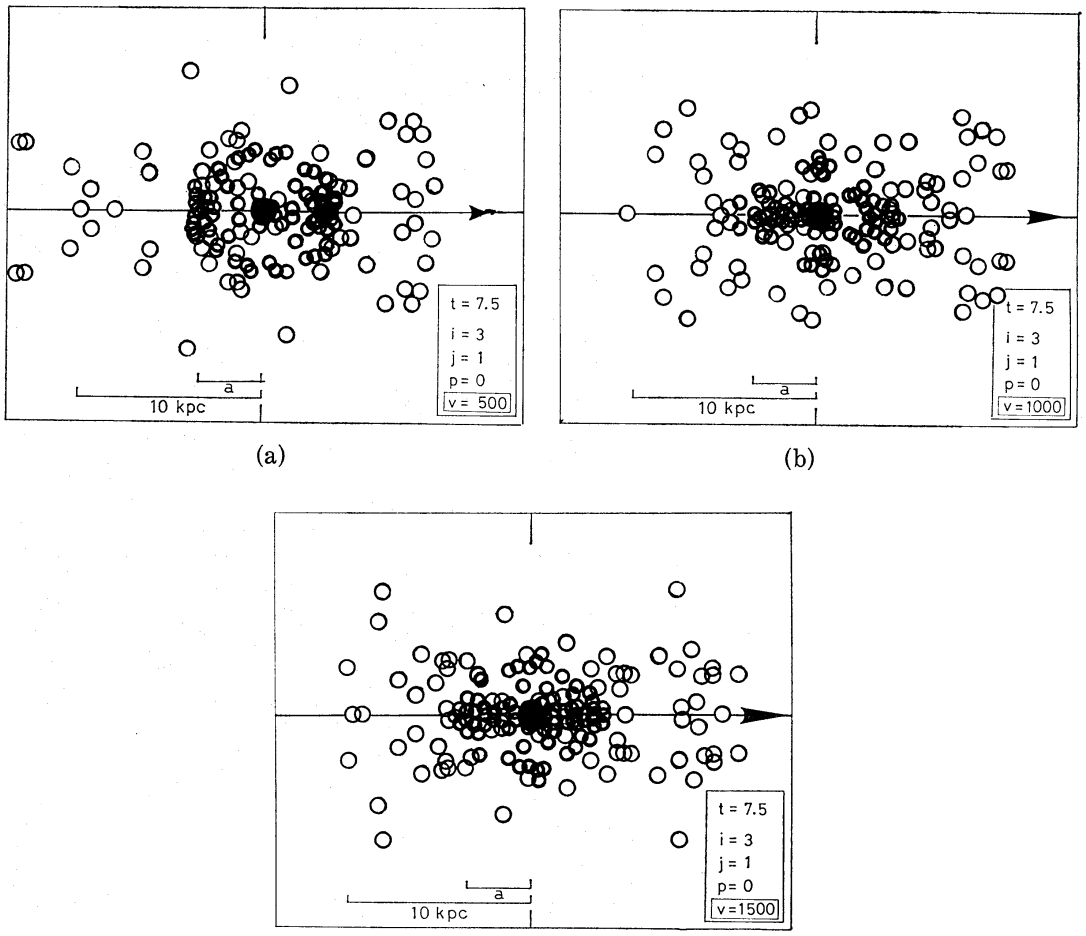

Fig. A5. Comparison of the particle distributions at $t=7.5\times10^7$ yr after a head-on collision. The relative velocities are assumed as 500,1000, and 1500 km s^{-1}, while other parameters are fixed as $(i, j; p)=(3, 1; 0$ kpc).

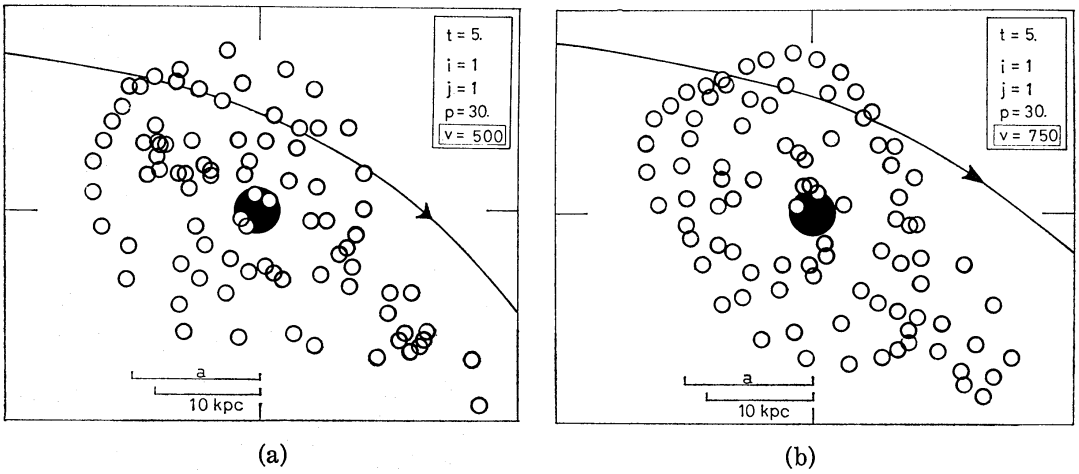

Fig. A6a-b. See the legend on the next page.

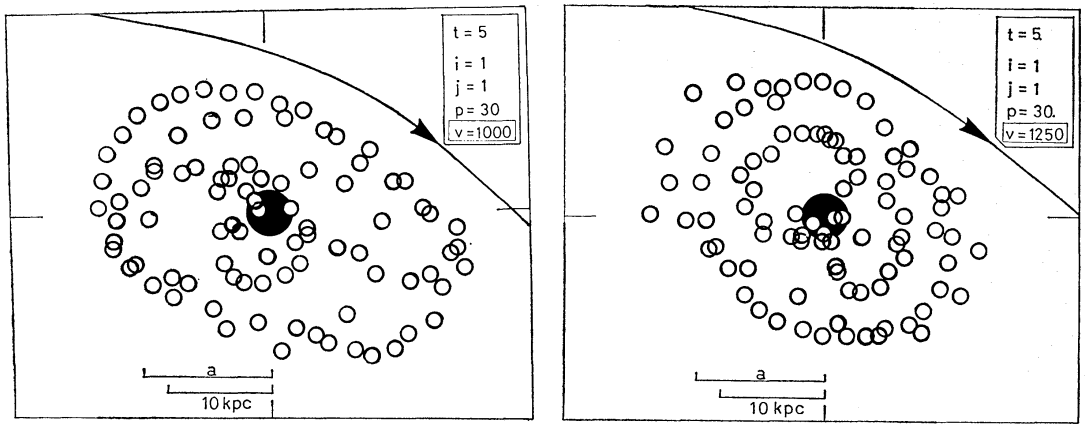

(c) (d)

Fig. A6. Same as figure A5, but at 5×10^7 yr after a distant encounter with the relative velocities 500, 750, 1000, and 1250 km s^{-1}. In these figures are indicated only the particles whose initial amplitudes were $\sim a_i$.

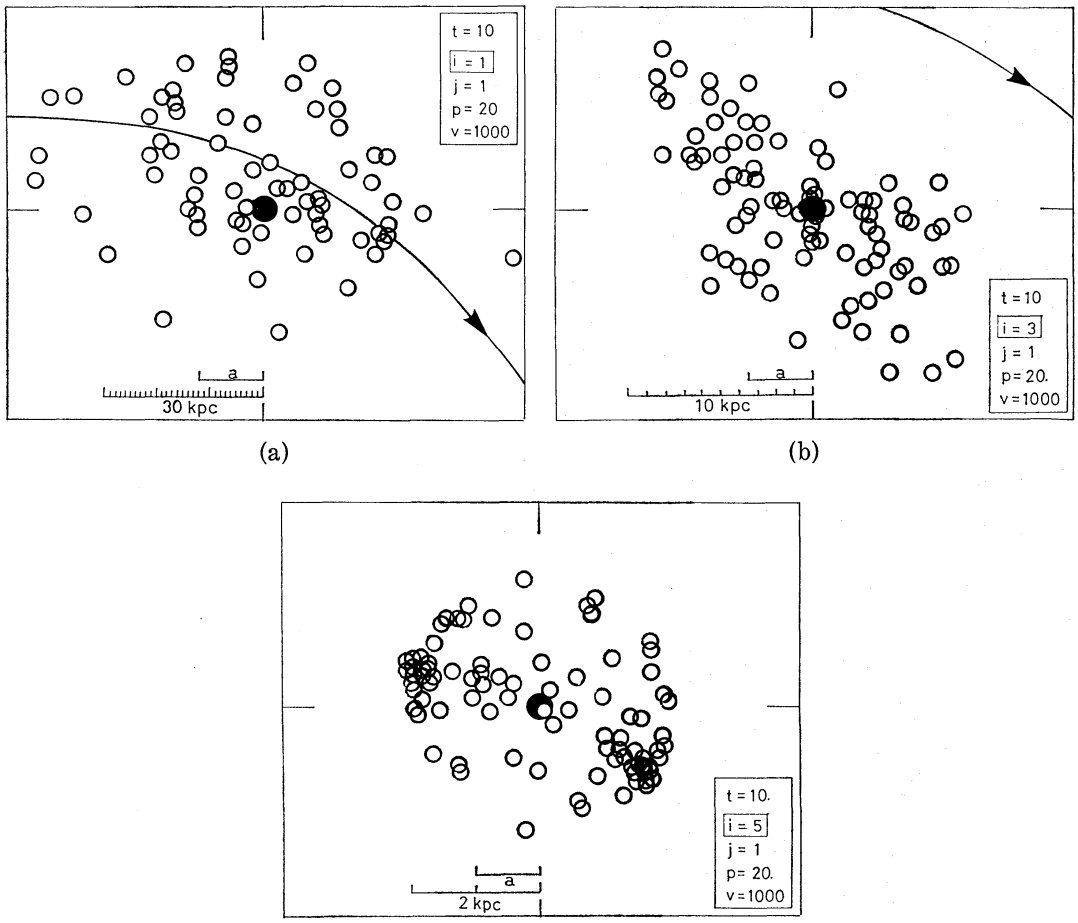

(a) (b)

(c)

Fig. A7. Comparison of the particle distributions in various model galaxies with masses of 10^{11}, 6.3×10^{11}, and $4\times10^{12}\,M_\odot$, or i=5, 3, and 1 at $t=10^8$ yr. In these figures are indicated only the particles whose initial amplitudes were $2a_i$. Other parameters are fixed as $(j;\ p,\ V)=(1;\ 20$ kpc, 1000 km s$^{-1})$.

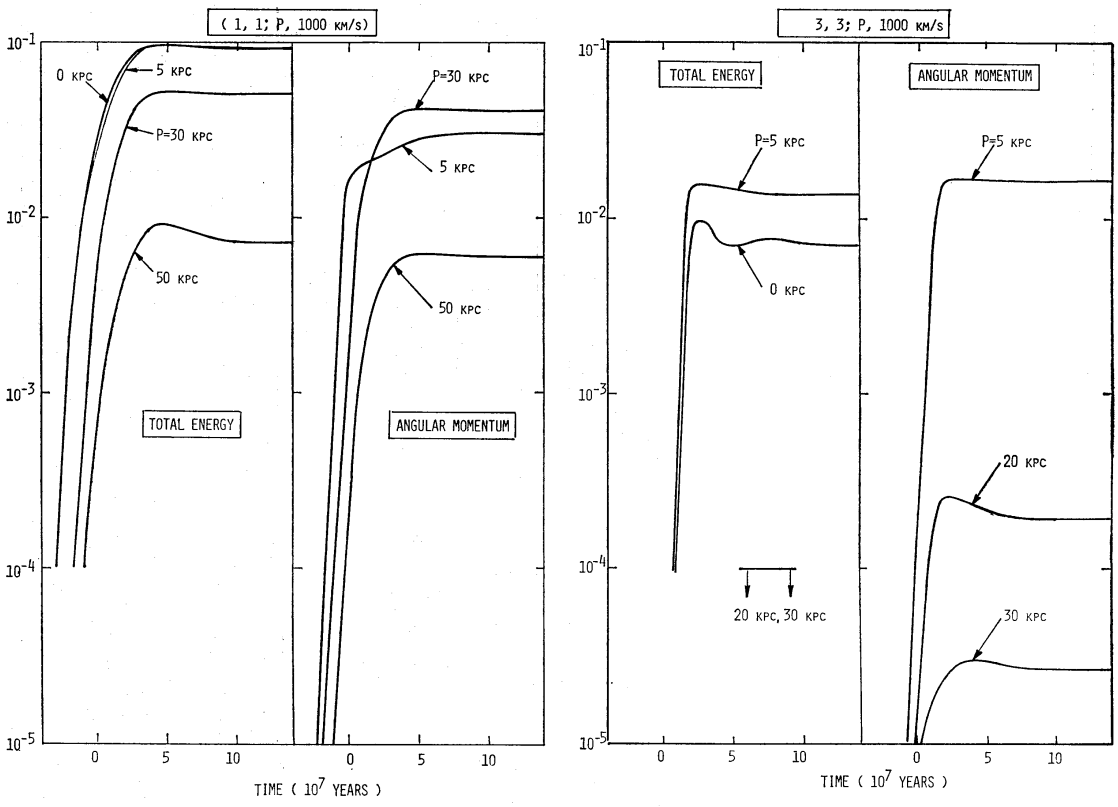

(a) (b)

Fig. A8. Time variations of total energy and angular momentum of the test particles. (a) $(i, j; V)=(1, 1; 1000 \text{ km s}^{-1})$ and (b) $(3, 3; 1000 \text{ km s}^{-1})$. The variations of energy and angular momentum are given normalized by their initial values before encounters.

that the outer portions ($|\boldsymbol{\rho}-\boldsymbol{\rho}_i|>a_i$) of massive galaxies are loosely bound as compared with the envelopes of less massive ones.

Total energy and angular momentum

Small fractions of the orbital angular momentum and the kinetic energy of two colliding galaxies are transferred to the test particles in each galaxy. Figures A8 and A9 show sudden increases (tidal shock) in the total energy and total angular momentum of the test particles. The energy and angular momentum are normalized respectively by their initial values, that is,

$$\sum_{k=1}^{K}(E_k-E_k^0)/|\sum_{k=1}^{K}E_k^0|$$

for energy, and

$$\frac{M_i|\sum_{k=1}^{K}(\boldsymbol{\rho}_k\times\boldsymbol{v}_k)|/K}{[M_iM_j/(M_i+M_j)]pV}$$

for angular momentum. Here E_k^0 and E_k denote the total energies of the k-th particle before and after the encounter, respectively. The vectors $\boldsymbol{\rho}_k$ and $\boldsymbol{v}_k$ denote the position vector and velocity referred to the perturbed galaxy, and K is the total number of the test particles.

Figures A10 and A11 are given to depict in which way the total energy

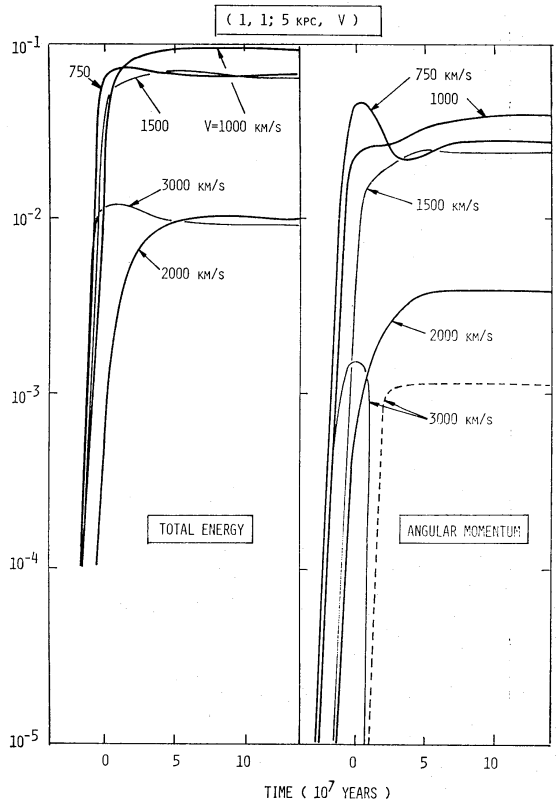

Fig. A9. Same as figure A8, but for various relative velocities. Other parameters are fixed as $(i, j; p)=(1, 1; 5$ kpc). The dashed line for $V=3000\,\mathrm{km\,s^{-1}}$ indicates a transient slight transfer of angular momentum from the particles to the orbital motion.

transfer and angular momentum transfer depend on the parameters p and V. We find that the latter is most efficient at $p=2a_i$. Also notable is that the transfer of energy is not so exactly described as $\Delta E\cong p^{-4}V^{-2}$ predicted in the impact approximation (Spitzer 1958), when $p<4a_i$ and $V<1000\,\mathrm{km\,s^{-1}}$.

These results suggest that the total energy and angular momentum of elliptical galaxies in the Coma cluster would increase in a cumulative way at successive encounters, which enhance the evaporation of stars from these galaxies and eventually form diffuse star clouds in intergalactic space.

Such evaporations may be efficient in massive ellipticals, the outer portion of which is, as already mentioned, loosely bound. In this context, it is worthwhile to note the existence of diffuse and massive galaxies, NGC 4874 and 4889, in the central region of the cluster (see, e.g., Welch and Sastry 1971).

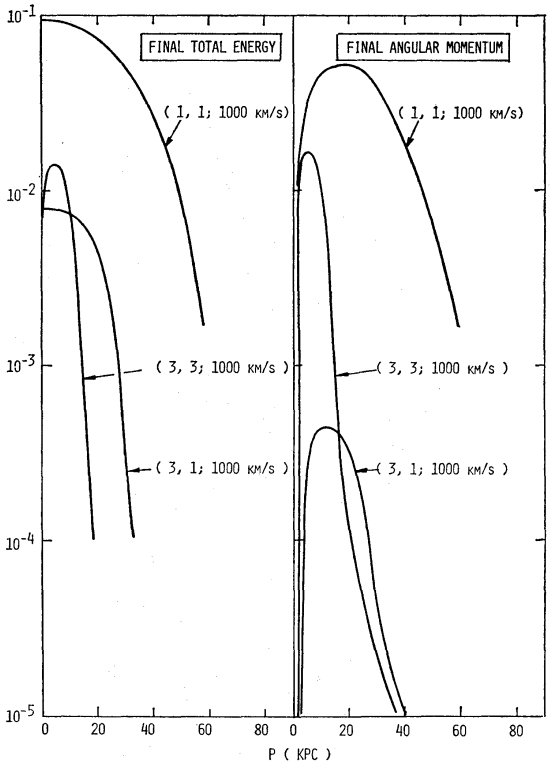

Fig. A10. Net increases in total energy and angular momentum as a function of the impact parameter. Some parameter combinations of $(i, j; V)$ are taken.

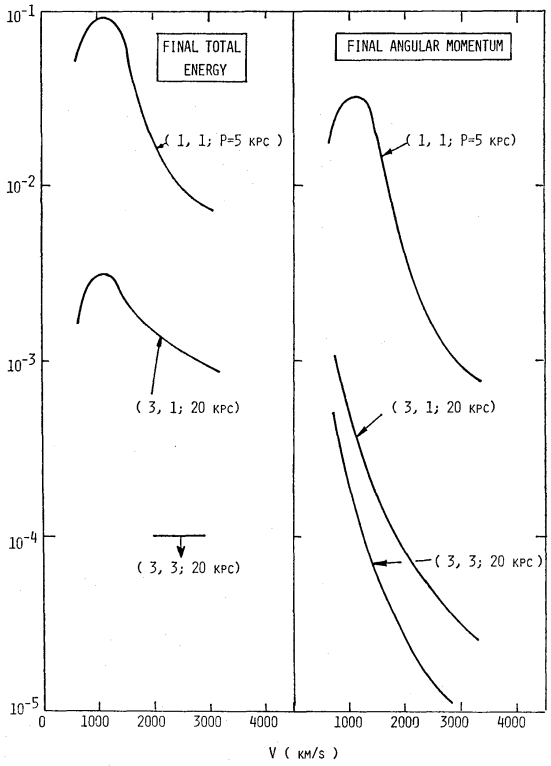

Fig. A11. Same as figure A10 but as a function of the relative velocity V. Three combinations of $(i, j; p)$ are taken.

References

Clutton-Brock, M. 1972, *Astrophys. Space Sci.*, **17**, 292.
Eneev, T. M., Kozlov, N. N., and Sunyaev, R. A. 1973, *Astron. Astrophys.*, **22**, 41.
Field, G. B. 1972, *Ann. Rev. Astron. Astrophys.*, **10**, 227.
Fish, R. A. 1964, *Astrophys. J.*, **139**, 284.
Fujimoto, M., and Sofue, Y. 1976, *Astron. Astrophys.*, **47**, 263.
Omer, G. C., Jr., Page, T. L., and Wilson, A. G. 1965, *Astron. J.*, **70**, 440.
Pfleiderer, J. 1963, *Z. Astrophys.*, **58**, 12.
Pfleiderer, J., and Siedentopf, H. 1961, *Z. Astrophys.*, **51**, 201.
Plummer, H. C., 1911, *Monthly Notices Roy. Astron. Soc.*, **71**, 460.
Rood, H. J. 1968, *Publ. Astron. Soc. Pacific*, **80**, 424.
Rood, H. J. 1969, *Astrophys. J.*, **158**, 657.
Rood, H. J., and Baum, W. A. 1967, *Astron. J.*, **72**, 398.
Rood, H. J., Page, T. L., Kintner, E. C., and King, I. R. 1972, *Astrophys. J.*, **175**, 627.
Spitzer, L. 1958, *Astrophys. J.*, **127**, 17.
Tarter, J., and Silk, J. 1974, *Quart. J. Roy. Astron. Soc.*, **15**, 122.
Toomre, A., and Toomre, J. 1972, *Astrophys. J.*, **178**, 623.
van den Bergh, S. 1969, *Nature*, **224**, 891.
Welch, G. A., and Sastry, G. N. 1971, *Astrophys. J.*, **169**, L3.
Wright, A. E. 1972, *Monthly Notices Roy. Astron. Soc.*, **157**, 309.
Yabushita, S. 1971, *Monthly Notices Roy. Astron. Soc.*, **153**, 97.
Zwicky, F. 1933, *Helvetica Phys. Acta*, **6**, 110.